Spontaneous Tumor Development in Bone Marrow Rescued DNA-PKcs[3A/3A] Mice Due to Dysfunction of Telomere Leading Strand Deprotection

Shichuan Zhang[1,2,6,7], **Shinji Matsunaga**[1,3,6], **Yu-Fen Lin**[1], **Brock Sishc**[1], **Zengfu Shang**[1], **Jiangdong Sui**[1], **Hung-Ying Shih**[1], **Yong Zhao**[4], **Oded Foreman**[5], **Michael D. Story**[1], **David J. Chen**[1], and **Benjamin PC. Chen**[1,7]

[1]Division of Molecular Radiation Biology, Department of Radiation Oncology, University of Texas Southwestern Medical Center at Dallas, Dallas, TX 75390

[2]Department of Radiation Oncology, Sichuan Cancer Hospital, Chengdu 610041, P.R. China

[3]Division of Molecular Pharmacology, Department of Pathophysiological and Therapeutic Science, Tottori University, Yonago 683–8504, Japan

[4]Key Laboratory of Gene Engineering of the Ministry of Education, Cooperative Innovation Center for High Performance Computing, School of Life Sciences, Sun Yat-sen University, Guangzhou 510006, P.R. China

[5]The Jackson laboratory, Sacramento, CA, US

Abstract

Phosphorylation of the DNA-dependent protein kinase catalytic subunit (DNA-PKcs) at the Thr2609 cluster is essential for its complete function in DNA repair and tissue stem cell homeostasis. This phenomenon is demonstrated by congenital bone marrow failure occurring in DNA-PKcs[3A/3A] mutant mice, which require bone marrow transplantation (BMT) to prevent early mortality. Surprisingly, an increased incidence of spontaneous tumors, especially skin cancer, was observed in adult BMT-rescued DNA-PKcs[3A/3A] mice. Upon further investigation we found that spontaneous γH2AX foci occurred in DNA-PKcs[3A/3A] skin biopsies and primary keratinocytes and that these foci overlapped with telomeres during mitosis, indicating impairment of telomere replication and maturation. Consistently, we observed significantly elevated frequencies of telomere fusion events in DNA-PKcs[3A/3A] cells as compared to wild type and DNA-PKcs knockout cells. In addition, a previously identified DNA-PKcs Thr2609Pro mutation, found in breast cancer, also induces a similar impairment of telomere leading end maturation. Taken together, our current analyses indicate that the functional DNA-PKcs T2609 cluster is required to

[7]To whom correspondence should be addressed: Shichuan Zhang, M.D., Ph.D., Department of Radiation Oncology, Sichuan Cancer Hospital, Chengdu 610041, P.R. China, Phone: 86-028-85420254, Fax: 86-028-85420116, zhangsc65@hotmail.com. Benjamin P.C. Chen, Ph.D., Department of Radiation Oncology, University of Texas Southwestern Medical Center at Dallas, 2201 Inwood Rd., Rm. NC7.206, Dallas, TX 75390-9187, USA, Phone: 214-648-1263, Fax: 214-648-5995, benjamin.chen@utsouthwestern.edu.
[6]These authors contributed equally to this work.

facilitate telomere leading strand maturation and prevention of genomic instability and cancer development.

Introduction

Non-homologous end joining (NHEJ) is the predominant pathway involved in DNA double strand break (DSB) repair in mammals. It is mediated by the fast binding of the Ku70/Ku80 homodimer from DNA-dependent protein kinase (DNA-PK) to the exposed DSB termini, followed by recruitment of the catalytic DNA-PKcs subunit to the broken ends[1]. Loading at the DSB ends promotes the kinase activity of DNA-PKcs and its autophosphorylation at various residues. DNA-PKcs phosphorylation at the Thr2609 cluster region is particularly critical for DSB repair and cellular resistance to ionizing radiation (IR) [2–4]. Although the Thr2609 cluster was initially identified *in vitro* upon DNA-PKcs activation [3, 5] and may be mediated by *trans* autophosphorylation *in vivo* [6], further examination revealed that IR-induced DNA-PKcs phosphorylation at the Thr2609 cluster is also regulated by the ataxia-telangiectasia mutated (ATM) kinase [2]. Additionally, following UV irradiation or under replication stress conditions, the Thr2609 cluster is rapidly phosphorylated by the ATM and Rad3-related (ATR) kinase [7], suggesting a crucial role in regulation of DNA-PKcs activity. This is consistent with the notion that phosphorylation at the Thr2609 cluster region induces a large conformational change in DNA-PKcs, disassembling the DNA-PK complex and releasing DNA-PKcs from DSBs [8].

Our findings in DNA-PKcs phosphorylation at the Thr2609 cluster have led us to develop a knock-in mouse model harboring three alanine substitutions at the mouse equivalent Thr2605 cluster (Thr2605A, Thr2634A, and Thr2643A, 3A mutation in brief) [9]. In sharp contrast to DNA-PKcs knock-out (DNA-PKcs$^{-/-}$) and DNA-PKcs deficient *scid* mice, homozygous DNA-PKcs$^{3A/3A}$ mice all died prematurely after birth due to congenital bone marrow failure and loss of hematopoietic stem cells (HSC, Lin-Sca-1$^+$c-Kit$^+$). Additional studies revealed that DNA-PKcs$^{3A/3A}$ embryos initially have similar proportions of HSCs in the e12.5 fetal liver. HSC pools fail to expand during e12.5–e16.5, when they are highly proliferative and undergo rapid expansion in fetal liver [10], prior to their migration to the newly formed bone marrow niches. Failure of DNA-PKcs$^{3A/3A}$ HSC expansion is likely due to a disability in resolving replication-associated DNA damage. This fact is further supported by an increase of apoptotic cell death in intestinal crypts where proliferating intestinal stem cells reside [9]. As expected, mouse embryonic fibroblasts (MEFs) derived from homozygous e13.5 DNA-PKcs$^{3A/3A}$ embryos were highly sensitive to irradiation (IR) similarly to DNA-PKcs$^{-/-}$ MEFs, as compared with wild type MEFs. In addition, DNA-PKcs$^{3A/3A}$ cells were sensitive to replication stressors, especially DNA interstrand crosslink (ICL) agents (e.g. cisplatin and mitomycin C). An increase in ICL sensitivity was not observed in DNA-PKcs$^{-/-}$ MEFs suggesting a gain-of-function effect of the DNA-PKcs^{3A} knock-in mutation. Consistently, DNA-PKcs$^{3A/3A}$ cells also display defects in the Fanconi Anemia (FA) pathway and homologous recombination (HR) mediated DSB repair, both known to be crucial in resistance and repair of ICL DNA lesions [11].

Additionally, DNA-PKcs[3A/3A] mice display a skin hyperpigmentation phenotype, indicating an increase of genotoxic stress in keratinocytes and an elevation of the p53 dependent response [12]. This occurs as the p53 null background alleviates both HSC loss and skin pigmentation phenotypes in DNA-PKcs[3A/3A] mice [9]. Congenital bone marrow failure and skin pigmentation are associated with dyskeratosis congenita (DC), a human bone marrow failure syndrome, characterized by defects in telomere maintenance [13, 14]. Similar phenotypes were also observed in mice with double knockouts of *protection of telomeres 1b* (*POT1b*) and *telomerase RNA* (*mTR*) genes [15, 16]. An increase in telomere fusions was previously reported in DNA-PKcs knockout mouse cells [17–19] as well as in the recently described DNA-PKcs kinase dead mutant mouse cells [20]. In addition, abolishing DNA-PKcs phosphorylation in the 2609 cluster, but not in the 2056 cluster, induces a significant increase in basal and radiation-induced telomere fusion events [21]. Taken together, these studies suggest that abolishing DNA-PKcs phosphorylation at the Thr2609 cluster might lead to telomere dysfunction. In the current study, we demonstrate that telomere maintenance is impaired in skin keratinocytes and MEFs derived from DNA-PKcs[3A/3A] mice. Our results indicate that the DNA-PKcs 3A mutation will cause telomere deprotection in newly synthesized leading strands (G-overhang) in M phase. Telomere-associated DNA damage responses are involved in HSC loss, skin pigmentation conditions, and increased tumor incidence found in DNA-PKcs[3A/3A] mice.

Results

Tumor-prone phenotype in bone marrow rescued DNA-PKcs[3A/3A] mice

Early mortality of DNA-PKcs[3A/3A] mice could be fully rescued by a previously published bone marrow transplantation (BMT) procedure [9]. Upon BMT rescue, DNA-PKcs[3A/3A] mice gained weight similarly to wild type mice (data not shown) with no obvious developmental abnormalities. However, spontaneous tumor development was found in mice as young as three-months old. A significant difference in tumor free survival was observed between BMT-rescued DNA-PKcs[3A/3A] mice and wild type control mice (P=0.0006, Fig 1A). Within a cohort of 32 BMT-rescued DNA-PKcs[3A/3A] mice with a complete life span and pathology analyses, 14 animals developed tumors in various tissues origins, including solid tumors (Table 1). This phenomenon was not observed in DNA-PKcs deficient *scid* mice even following γ-irradiation treatment [22]. Furthermore, rescued DNA-PKcs[3A/3A] mice displayed a relatively high incidence of skin squamous cell carcinoma (SCC), as compared with spontaneous and γ-ray induced tumor spectrum identified in *scid* mice (Table 1 and Fig 1B). These data correlate with our previous report of a p53-dependent skin hyperpigmentation character in DNA-PKcs[3A/3A] mice [9]. Our observations led us to further explore the underlying mechanism of skin abnormality in DNA-PKcs[3A/3A] mice.

Increase of mitosis-associated genotoxic stress in DNA-PKcs[3A/3A] keratinocytes

Skin hyperpigmentation has been characterized as a sign of the genotoxic effect caused by an elevation of the p53 dependent mechanism [12]. In agreement with these findings, the skin hyperpigmentation phenotype of DNA-PKcs[3A/3A] mice was eliminated upon crossing with p53 knockout mice [9]. To further characterize the underlying mechanism of this genotoxic effect, skin keratinocytes were freshly isolated from postnatal day one (P1) skin biopsies of

DNA-PKcs$^{3A/3A}$ mutant and wild type pups. Cells were further cultured for immunofluorescence staining against γH2AX, a general marker for DNA damage response. Significant and spontaneously occurring γH2AX foci were found in the DNA-PKcs$^{3A/3A}$ keratinocytes but not in wild type cells (Fig 2A). Furthermore, spontaneous γH2AX foci were primarily observed in mitotic cells that were positively stained with phospho-histone 3 (pH3). No γH2AX foci were detected in DNA-PKcs$^{3A/3A}$ keratinocytes during G2 phase (with sporadic staining pattern of pH3) or prometaphase. Significant induction of γH2AX was found in metaphase and lasted till anaphase (Fig 2A).

To confirm the same phenomena *in vivo*, skin specimens harvested from wild type and DNA-PKcs$^{3A/3A}$ pups were sectioned and stained by immunofluorescence. As shown in Fig 2B, an increase of γH2AX staining was observed in skin sections of DNA-PKcs$^{3A/3A}$ mice as compared to wild type littermates. Furthermore, γH2AX staining overlapped exclusively with pH3 positive mitotic cells sparsely distributed in the basal layer of the epithelium. Over one hundred pH3 positive keratinocytes were examined from the DNA-PKcs$^{3A/3A}$ skin sections and all concomitantly stained with γH2AX. In contrast, no γH2AX positive cells were found in the pH3 negative DNA-PKcs$^{3A/3A}$ cells or in the wild type skin sections.

Localization of mitotic γH2AX foci at telomeres in DNA-PKcs$^{3A/3A}$ cells

Staining of γH2AX in mitotic DNA-PKcs$^{3A/3A}$ keratinocytes was largely concentrated at chromosomes ends or in the telomere region. To validate this hypothesis, primary DNA-PKcs$^{3A/3A}$ skin keratinocytes were immunostained against γH2AX and telomeric repeat factor 1 (TRF1), one of the key components of the telomere protective shelterin complex [23]. Our analysis revealed that mitosis-induced γH2AX foci significantly overlapped with TRF1 staining in DNA-PKcs$^{3A/3A}$ keratinocytes (Fig 3A). On average, over 30 γH2AX foci (31.33 ± 9.11) were counted in each mitotic DNA-PKcs$^{3A/3A}$ keratinocyte, a significantly higher number than that observed during interphase (0.7 ± 2.00) (Fig 3B). Furthermore, the majority of the γH2AX foci overlapped with TRF1 foci during mitosis ($88.0\% \pm 5.0\%$) as compared to interphase ($15\% \pm 18.5\%$) (Fig 3C).

Increase of spontaneous γH2AX foci was also found in hematopoietic stem cells (HSC) freshly isolated from e12.5–e14.5 fetal livers of DNA-PKcs$^{3A/3A}$ embryos [9]. To determine whether spontaneous γH2AX foci also occurred in HSCs during mitosis, freshly isolated fetal liver HSCs were subjected to IF staining against γH2AX and pH3. As shown in Fig 3D, pH3 positive HSCs displayed significant γH2AX foci at chromosome ends. Furthermore, mitotic γH2AX foci overlapped with TRF1 staining in DNA-PKcs$^{3A/3A}$ HSCs showing an inverse correlation in their intensities (Fig 3E). These results validated our observation that spontaneous γH2AX induction occurs in telomeres during mitosis in DNA-PKcs$^{3A/3A}$ cells.

Telomere dysfunction in DNA-PKcs$^{3A/3A}$ cells

Independent studies have reported a significant increase of telomere fusions in DNA-PKcs knockout (DNA-PKcs$^{-/-}$) mouse cells, indicating a role of DNA-PKcs in telomere protection [17–19]. To determine further escalation of telomere dysfunction in DNA-PKcs$^{3A/3A}$ cells, early passages of primary mouse embryo fibroblast (MEF) cultures were processed for

mitotic spread, followed by fluorescence in situ hybridization (FISH) with C- or G-rich telomeric peptide–nucleic acid probes (TelC or TelG PNA probes, respectively). As shown in Fig 4A, a significant increase in telomere fusion was found in DNA-PKcs[3A/3A] MEFs. We observed that 46.0% ± 2.8% of DNA-PKcs[3A/3A] MEFs displayed telomere fusions, which was significantly higher compared to wild type MEFs (1.0% ± 1.4%) cells or DNA-PKcs^{−/−} MEFs (20.0% ± 5.7%) (Fig 4B). Our analyses also revealed frequencies of telomere fusion per chromosome in DNA as follows: PKcs[3A/3A] (1.46 ± 0.25), wild type (0.03 ± 0.04), and DNA-PKcs^{−/−} (0.34 ± 0.19) cells (Fig 4C, 4D).

To determine whether an increase in telomere fusions in DNA-PKcs[3A/3A] cells is due to telomere erosion and length shortening, telomere FISH images were subjected to semi-quantitative FISH (Q-FISH) analysis [24]. Q-FISH analysis revealed no overall reduction of telomere length in DNA-PKcs[3A/3A] cells as compared to wild type cells (Fig 4E). This notion was further supported by pulse-field gel electrophoresis (PFGE) analysis, which directly measures telomere length from genomic DNA. Results showed no significant difference in telomere length between DNA-PKcs[3A/3A] and wild type cells (Fig 4F), suggesting that telomere length shortening does not occur in DNA-PKcs[3A/3A] cells.

Leading strand specific telomere deprotection in DNA-PKcs[3A/3A] cells

To further elucidate the mechanism of telomere dysfunction in DNA-PKcs[3A/3A] cells, primary skin fibroblasts were immunostained against γH2AX in conjunction with telomere FISH analysis. We observed that almost all mitosis-generated γH2AX foci in DNA-PKcs[3A/3A] cells overlapped with telomere FISH staining (Fig 5A). Furthermore, the majority of chromosomes displayed one or two γH2AX foci at the opposite end of each sister chromatid (Figs 5A, 5B), either at the leading or lagging strand telomeres. To determine the origin of γH2AX formation, leading and lagging strands were differentiated through chromosome orientation fluorescence in situ hybridization (CO-FISH) analysis. In CO-FISH newly synthesized telomere DNA nucleotide analogs (which include BrdU/BrdC) can be enzymatically removed to allow distinction between leading and lagging strand telomere synthesis [25]. CO-FISH analysis revealed that γH2AX foci in DNA-PKcs[3A/3A] cells predominantly overlapped with the TelG probe (Fig 5D), representing leading strand telomere synthesis. This overlap was not observed with the TelC probe, representing lagging strand telomere synthesis (Fig 5C). The presence of the γH2AX signal at the leading strand telomere synthesis was significantly higher in DNA-PKcs[3A/3A] cells as compared to wild type or DNA-PKcs^{−/−} cells (Fig 5E).

A Thr2609Pro missense variant of human DNA-PKcs causes deprotection in leading strand telomeres

Our analyses revealed that DAN-PKcs phosphorylation at the Thr2609 cluster is required for telomere protection especially in leading strand telomere synthesis. Defects in DNA-PKcs Thr2609 cluster phosphorylation may result in telomere dysfunction and genome instability. Somatic mutations in DNA-PKcs encoding the *PRKDC* gene have been reported among human cancers (see review in Hsu et al [26]). A c.7825A>C variant, resulting in a proline substitution at Thr2609 (p.Thr2609Pro), was identified from a breast cancer biopsy specimen [27]. To test whether this p.Thr2609Pro missense variant would lead to a phenotype

similar to the DNA-PKcs[3A] mutation, DNA-PKcs deficient CHO-V3 cells were complemented with full length human DNA-PKcs harboring the Thr2609Pro (T2609P) mutation. V3-T2609P cells were more sensitive to ionizing radiation than V3 cells expressing wild type DNA-PKcs or mutant DNA-PKcs carries alanine substitution at Thr2609 (T2609A) (Fig 6A and Supplemental Fig S1). In addition, V3-T2609P cells displayed hypersensitivity toward mitomycin C (Fig 6B) as observed in cells lacking the functional Thr2609 cluster [9, 28]. These data suggest that the T2609P single mutation (but not the T2609A single mutation) could disrupt normal functioning of the Thr2609 cluster in DNA damage repair.

Similarly to mouse DNA-PKcs[3A/3A] cells, we observed that V3-T2609P cells displayed defects in telomere protection. When V3-T2609P cells were immunostained against γH2AX and pH3, the majority of pH3 positive V3-T2609P cells (>87%) showed significant γH2AX foci formation as compared to wild type CHO AA8 cells or V3 cells complemented with wild type DNA-PKcs (Figs 6C–6E). Furthermore, we observed a similar pattern in CO-FISH analysis between V3-T2609P cells (Fig 6F) and mouse DNA-PKcs[3A/3A] cells (Fig 5C), suggesting that the T2609P DNA-PKcs mutant also causes leading strand telomere deprotection.

Discussion

We have previously described the DNA-PKcs[3A] mouse model, characterized by a deficiency in functional Thr2605 (human Thr2609) phosphorylation cluster and congenital bone marrow failure (CBMF) due to an impairment in fetal liver HSCs expansion [9]. Our analyses also revealed additional underlying mechanisms including defects in multiple DNA repair pathways, suggesting a versatile role of the Thr2609 cluster in DNA damage repair. In the current study, we demonstrate induction of spontaneous γH2AX in proliferating DNA-PKcs[3A/3A] cells during mitosis (Figs 2, 3). This mitosis-specific surge of γH2AX appeared predominantly at telomeres, and correlated with an increase of telomere fusion events but not telomere shortening in DNA-PKcs[3A/3A] cells (Fig 4). Using CO-FISH analysis in conjunction with immunostaining, we further demonstrated leading strand-specific telomere end capping dysfunction at newly replicated telomeres in DNA-PKcs[3A/3A] cells (Fig 5). This mitosis-associated γH2AX formation and telomere dysfunction were observed across different cell types including skin keratinocytes or fibroblasts, MEFs, and fetal liver HSCs. The same phenomenon was observed in DNA-PKcs deficient CHO-V3 cells expressing the Thr2609Pro missense DNA-PKcs mutant (Fig 6). Thus, our studies reveal that DNA-PKcs phosphorylation at the Thr2609 cluster is crucial for newly synthesized leading strand telomere maturation and protection, which would otherwise result in telomere-associated DNA damage response. This could explain various pathophysiological characters including carcinogenesis in DNA-PKcs[3A/3A] mice.

Telomere dysfunction and skin pigmentation are the key phenotypic signs of dyskeratosis congenita (DC), a typical manifestation of human CBMF; furthermore, the DC disease gene dyskerin/DKC1 is a known stabilizer the telomerase complex, critical for its function *in vivo* [13, 14]. Based on our analyses, it is conceivable that mutations in the DNA-PKcs *PRKDC* gene could be present among DC patients. The involvement of DNA-PKcs in telomere

maintenance has been investigated mostly in DNA-PKcs knockout mouse models. Independent studies reported an increase of telomere fusion in mouse DNA-PKcs$^{-/-}$ cells independent of telomere shortening, a phenotype suggestive that DNA-PKcs is mainly involved in telomere capping, not telomere length maintenance[18, 19]. Similarly, we did not observe significant changes in telomere length (Fig 4F) or telomerase activity in DNA-PKcs$^{3A/3A}$ cells (Supplemental Fig 2S), although subtle telomere shortening and accelerated aging phenotypes may be present in DNA-PKcs deficient mice [29, 30]. Our study reveals that significant increase of telomere fusions was found in DNA-PKcs$^{3A/3A}$ cells than in DNA-PKcs$^{-/-}$ cells. Dysregulation of telomere is also found in kinase dead mutant DNA-PKcs$^{KD/KD}$ mouse cells [20]. Approximately 40% of DNA-PKcs$^{KD/KD}$ metaphase spreads display telomere abnormalities [20], and similar telomere incident was observed in DNA-PKcs$^{3A/3A}$ spreads. These results indicate that both DNA-PKcs kinase activity and Thr2609 cluster phosphorylation are crucial for telomere protection in mouse cells. In comparison, DNA-PKcs knockout in human cells results in a more severe telomere phenotype since telomere shortening was found not only in homozygous cells but also in heterozygous cells [31]. These data suggest that human DNA-PKcs plays a more critical role in telomere protection than mouse DNA-PKcs deficiency, a phenotype potentially due to the lack of observable telomerase activity in non-cancer human cells. Thus, DNA-PKcs^{3A} knock in mice represent a better mouse model to further delineate physiological functions of DNA-PKcs including its role in telomere protection and maintenance. The leading strand telomere deprotection characteristic also explains the significant increase of telomeric fusion in DNA-PKcs$^{3A/3A}$ cells and severe phenotypic development in DNA-PKcs$^{3A/3A}$ mice as compared to the DNA-PKcs null background.

Deprotection of leading strand telomeres has been previously observed in mouse DNA-PKcs$^{-/-}$cells. Bailey et al identified telomeric chromatid concatenates (TCCs) in mouse DNA-PKcs$^{-/-}$cells; although incidents were quite low (14 TCCs among a total of 850 cells scored), all TCCs identified were leading-to-leading strand fusions [17]. Consistent with these studies, our results demonstrated that leading strand telomere end-capping dysfunction manifests in DNA-PKcs$^{3A/3A}$ cells as evidenced by the formation of γH2AX foci predominantly in leading telomeres during mitosis. It is possible that the mutant DNA-PKcs^{3A} protein may interfere with the assembly of the telomere protective capping structure (Shelterin/telosome) at the newly replicated leading strand telomeres. We notice that the high incident of telomere abnormalities was not observed in our previous study [9]. The difference likely is due to different techniques applied to score chromosomal aberrations from metaphase spreads. Sensitive and telomere specific FISH techniques were applied throughout this investigation. The increase of telomeric fusions in DNA-PKcs$^{3A/3A}$ cells is also supported by telomere-associated γH2AX foci formation and a previous report that expression of Thr2609 cluster-mutant DNA-PKcs results in telomere dysfunction and telomere-DSB fusion [21].

Mechanisms involved in telomere protection, telomere DNA replication and subsequent recapping of newly replicated daughter telomeres are still not completely understood. Emerging evidence indicates that the leading strand telomere exploits different strategies, including the use of the lagging strand and shielding itself following replication[32, 33]. In late S-phase, lagging strand telomeres form a 3′ single stranded, G-rich overhang due to the

removal of the RNA primer in the terminal Okazaki fragment and failure to position the fragment at the chromosome terminus. In contrast, leading strand telomeres form near blunt ends or carry a few nucleotides in overhang after replication. Leading strand telomeres may also gain the G-rich overhang through processing steps in late S/G2 phase [33]. Additionally, a late processing event takes place in G2/M phase to position the terminal nucleotides of the leading C-strand for final maturation of G-overhang at the leading strand telomeres [33, 34]. The G-overhang can be produced through telomerase-dependent telomere elongation [32, 33]. Alternatively, it could be generated through an end-resection mechanism mediated by Snm1b/Apollo, a TRF2-interacting exonuclease, for G-overhang production at leading-end telomeres [35]. Due to this end processing procedure, there is a delay of G-overhang completion at the leading daughter telomeres, whereas the G-overhang at the lagging daughter telomeres immediately mature following replication [33].

The delay of G-overhang completion at newly replicated leading strand telomeres explains the decrease in chromatin binding of POT1 in G2 phase, the single-stranded DNA (ssDNA) binding component of the shelterin complex, and the increase of DSB repair proteins loading in telomeric DNA[36]. It has been postulated that the association of DSB repair proteins at G2 telomeres is required for the recruitment of the processing machinery to produce the G-overhang in leading daughter telomeres. Although the dynamic association of DNA-PK complex with telomeres during G2 is still unclear, we have recently reported that DNA-PK dependent hnRNP-A1 phosphorylation is required for the RPA-to-POT1 switch and telomere capping in newly replicated telomeres [37]. Additionally, the presence of DNA-PK complex may prevent telomere termini from being targeted by homologous recombination (HR), as knockout of the Ku80 gene in human cells results in massive telomere loss due to HR mediated t-circles and telomere rapid deletion[38]. In contrast, excess or dysfunction of the DNA-PK complex may cause telomere fusion production. The regulation of the DNA-PK complex likely relies on proper and timely DNA-PKcs phosphorylation at the Thr2609 cluster, which induces a conformational change in DNA-PKcs and its dissociation from the Ku/DNA termini [8]. This dynamic allows an orderly end processing and G-overhang maturation in the leading daughter telomeres. Mutations in DNA-PKcs Thr2609 phosphorylation may prolong the occupation of the DNA-PK complex in the telomere termini resulting in γH2AX foci formation. This notion is supported by our unpublished result on the phospho-blocking Thr2609Pro mutant DNA-PKcs which displays a distinctive protein degradation pattern, in limited proteolysis assay (when compared to wild type DNA-PKcs). These results suggest that mutations in the Thr2609 cluster interfere with conformational changes in DNA-PKcs and in the dynamic association of the DNA-PK complex.

Telomere-associated γH2AX foci were identified in cells following prolonged mitotic arrest due to the dissociation of TRF2 from telomeres and degradation of telomeric G-overhang, triggering ATM-dependent γH2AX signaling in telomeres[39]. In this setting, the appearance of γH2AX foci becomes evident only after hours from mitotic arrest. This delay in mitosis was not observed in DNA-PKcs$^{3A/3A}$ cells as similar mitotic indexes were measured in wild type, DNA-PKcs$^{-/-}$, and DNA-PKcs$^{3A/3A}$MEFs (data not shown). It is still uncertain if prolonged mitosis arrest preferentially induces deprotection in leading telomeres as observed in DNA-PKcs$^{3A/3A}$ cells. Although telomere deprotection is likely the common denominator

for this telomere-associated DNA damage response, the DNA-PKcs[3A] mutant protein may still trigger abnormal ATM signaling in mitosis. For example, DNA-PKcs and TRF2 cooperate to facilitate telomere loading of TRF2 and deter telomere fusion through an NHEJ independent mechanism [40, 41]. Since TRF2 is needed to minimize ATM kinase activation at telomeres[42], it is possible that the DNA-PKcs[3A] mutation attenuates telomere association of TRF2 or alleviates TRF2-dependent inhibition of ATM, consequently leading to the formation of telomere-associated γH2AX foci. Nonetheless, differential loading of TRF2 or shelterin complex in leading telomeres versus the lagging telomeres due to the distinctive sizes of their G-overhang still needs to be clarified [33].

Full activation of the DNA damage response in M phase is normally suppressed due to the absence of key components including 53BP1 and RNF8 [43]. It has been proved that DNA breakage in mitosis, including telomere associated DNA damage, is epigenetically marked by γH2AX and subsequently repaired in G1 phase [39, 44, 45]. The outcome of this rescue attempt could be due to either faithful repair of the DNA lesions, genomic instability, or cell death. In DNA-PKcs[3A/3A] mice, the fate of cells harboring telomere damage also varies depending on cell type and tissue origin. Hematopoietic stem cells undergo apoptosis when they enter the fast cycling stage in fetal liver [46]. In contrast, keratinocytes are not removed from the epidermis as there is no increased apoptosis either in situ or under culture conditions detected in DNA-PKcs[3A/3A] cells (data not shown). Nonetheless, DNA damage is elicited in these cells as shown by increased melanin accumulation in the skin of DNA-PKcs[3A/3A] mice. HSC apoptosis and increased melanin accumulation in keratinocytes were proved to be associated with p53 activation [9], as a direct consequence of the DNA damage response. Increased γH2AX foci were not observed in S and G2 phases of DNA-PKcs[3A/3A] keratinocytes, thus telomere deprotection in M phase is likely the major DNA damage stressor of the DNA-PKcs[3A/3A] mutation.

The current studies revealed that defects in DNA-PKcs phosphorylation at the Thr2609 cluster jeopardize telomere protection and homeostasis maintenance. Our results indicate that newly replicated telomeres, either in late G2 or M phase, will be recognized and occupied transiently by the DNA-PK complex. The ablation of DNA-PKcs phosphorylation will hamper the sequential processing of leading strand telomeres resulting in persistent DNA damage signaling and γH2AX foci formation in telomeres during mitosis. Importantly, the Thr2609Pro mutation identified from human breast cancer elicits the same cellular phenotype as the DNA-PKcs[3A] knock in mutation in mouse. These findings demonstrate the oncogenic effect due to a dysfunction of DNA-PKcs phosphorylation, warranting future investigations on the mechanistic link to pathological progression of CBMF diseases and cancer.

Materials and Methods

Spontaneous tumor development in DNA-PKcs[3A/3A] mice

Bone marrow transplantation of DNA-PKcs[3A/3A] mice was conducted as previously described[9]. BMT rescued DNA-PKcs[3A/3A] mice and wild type littermates were maintained and monitored for up to 24 months. Tumor-bearing mice were euthanized for tumor harvesting. Tumor samples were fixed with 4% neutralized paraformaldehyde for 24 hours,

processed for paraffin sectioning, and stained with hematoxylin-eosin according to standard protocol. After staining, tumor slides were examined by a veterinary pathologist, Dr. Foreman at the Jackson Laboratory. All animal procedures were conducted according to UTSW Institutional Animal Care and Use Committee-approved guidelines for animal welfare. A total of 32 BMT mice and 14 wild type mice were included in survival analysis. No randomization and blinding was applied in this study

Cell lines and treatment

Primary and SV-40 transformed MEFs from E13.5 embryos were cultured in alpha minimum essential medium supplemented with 10% fetal calf serum and penicillin/ streptomycin. MEFs were maintained in a 37°C humidified atmosphere with 3% O_2 and 10% CO_2. Primary keratinocytes were derived from tail skin. Briefly, skin flaps were treated with dispase (Sigma, St. Louis, MO) overnight in 4°C. Keratinocyte sheets were separated from the dermis and digested with trypsin (Sigma, St. Louis, MO). A single cell suspension was prepared and plated in conditional keratinocyte culture medium (Life Technologies, Carlsbad, CA). All cell cultures have been routinely tested mycoplasma contamination. Fetal liver hematopoietic stem cells (HSCs) isolation was performed as previously described[9].

Immunohistochemistry and immunofluorescence staining

Isolated HSCs were spread on glass slides using a CytoSpin4 centrifuge (Thermo Scientific, Waltham, MA). For immunofluorescence staining, cells were grown on poly-D-lysine–coated culture slides (BD Pharmingen, San Diego, CA), washed in PBS, fixed in PBS containing 4% paraformaldehyde, permeabilized in 0.5% Triton X-100, and blocked in PBS containing 5% bovine serum albumin. Cells were incubated with indicated primary antibodies for 2 hours at room temperature, washed with PBS, and incubated with Alexa-568 and Alexa-488-conjugated secondary antibodies for 1 hour (Life Technologies, Carlsbad, CA). Cells were then washed with PBS and mounted in Vectashield mounting medium with 4,6-diamidino-2-phenylindole (Vector Labs, Burlingame, CA). Images were acquired from a Zeiss AxioImager M2 microscope system equipped with a Plan-Apochromat 63×/NA 1.40 objective, an AxioCamMRm CCD camera, and AxioVision software (Carl Zeiss, Oberkochen, Germany). Anti-γH2AX (05-636, EMD Millipore, Billerica, MA) and anti-phospho-histone H3 (06-570, EMD Millipore, Billerica, MA) antibodies were purchased from the indicated vendors. The anti-TRF1 was a kind gift from Dr. Titia de Lange. Results presented in figures are representative examples for at least two replicated experiments using different cell lines or mice. The exact n number is documented in figure legends.

Telomere fluorescence in situ hybridization (FISH) and combination with γH2AX immunofluorescence staining

Fluorescence in situ hybridization (FISH) was performed in telomeres as previously described [37]. Quantitative FISH (Q-FISH) of relative telomere lengths was analyzed by the TFL-Telo image analysis software program [47]. Chromosome orientation fluorescence in situ hybridization (CO-FISH) was performed as previously described [9, 48]. For co-immunostaining with γH2AX, immunofluorescence staining of γH2AX was performed prior to the CO-FISH procedure. In brief, cells were cultured in medium containing 7.5 mM

of BrdU and 2.5 mM of BrdC for 16–20 hour, and treated with 0.2 μg/ml colcemid for the final 30 minutes. Cells were harvested and prepared for CytoSpin to make chromosome spread slides. Slides were immunostained with anti-γH2AX antibody and a fluorescein-labeled secondary antibody. After fixation with 4% paraformaldehyde, slides were dehydrated and dried out for modified CO-FISH assay. Cells were incubated with peptide nucleic acid (PNA) telomere probes (Panagene Inc., Daejeon, South Korea) in a 83°C oven for 3–5 minutes and returned to room temperature for hybridization for 2 additional hours. After being washed and dehydrated, slides were mounted and saved for analysis.

Southern blot hybridization to measure telomere length

Genomic DNA was isolated with a phenol/chloroform method and digested with Hinf I and Rsa I (New England Biolabs, Ipswich, MA). After digestion, DNA samples were resolved on a 0.7% agarose gel using a CHEF-DR II pulse field gel electrophoresis system (Bio-Rad, Hercules, California). The denatured and dried gel was hybridized with ^{32}P-labeled (CCCTAA)x3 oligonucleotides and exposed to a phosphor imager screen and analyzed by Typhoon 9410 scanner (GE Healthcare, Piscataway, NJ).

Statistical analysis

For survival analysis, the sample size was determined based on formula suggested by Schoenfeld [49] with an estimated relative risk of 5, estimated median survival of 12 months for DNA-PKcs$^{3A/3A}$ group, and a total of two year follow-up. P-values for survival curves were determined from the Kaplan–Meier survival curves by use of the log-rank test. For comparisons of quantitative data among groups, multiple samples for each group were included and analyzed with Wilcoxon rank-sum test (compare two groups) and Kruskal-Wallis test (compare multiple groups). Same experiment was replicated at least once using different cell lines or mice. The number (N) for each group and batch number of experiments are indicated in the corresponding figure legends. P-values <0.05 were taken as statistically significant. For comparison among three groups, P-values were adjusted to 0.0167. Sigmaplot 11 software (Systat Software, Chicago, IL) was used for statistical analysis. Survival curves and histogram figures were generated by GraphPad Prism software (GraphPAD Software, San Diego, CA).

Supplementary Material

Refer to Web version on PubMed Central for supplementary material.

Acknowledgments

References

1. Davis AJ, Chen DJ. DNA double strand break repair via non-homologous end-joining. Translational cancer research. 2013; 2:130–143. [PubMed: 24000320]

2. Chen BP, Uematsu N, Kobayashi J, Lerenthal Y, Krempler A, Yajima H, et al. Ataxia telangiectasia mutated (ATM) is essential for DNA-PKcs phosphorylations at the Thr-2609 cluster upon DNA double strand break. J Biol Chem. 2007; 282:6582–6587. [PubMed: 17189255]

3. Ding Q, Reddy YV, Wang W, Woods T, Douglas P, Ramsden DA, et al. Autophosphorylation of the catalytic subunit of the DNA-dependent protein kinase is required for efficient end processing during DNA double-strand break repair. Mol Cell Biol. 2003; 23:5836–5848. [PubMed: 12897153]

4. Reddy YV, Ding Q, Lees-Miller SP, Meek K, Ramsden DA. Non-homologous end joining requires that the DNA-PK complex undergo an autophosphorylation-dependent rearrangement at DNA ends. J Biol Chem. 2004; 279:39408–39413. [PubMed: 15258142]

5. Chan DW, Chen BP, Prithivirajsingh S, Kurimasa A, Story MD, Qin J, et al. Autophosphorylation of the DNA-dependent protein kinase catalytic subunit is required for rejoining of DNA double-strand breaks. Genes Dev. 2002; 16:2333–2338. [PubMed: 12231622]

6. Meek K, Douglas P, Cui X, Ding Q, Lees-Miller SP. trans Autophosphorylation at DNA-dependent protein kinase's two major autophosphorylation site clusters facilitates end processing but not end joining. Mol Cell Biol. 2007; 27:3881–3890. [PubMed: 17353268]

7. Yajima H, Lee KJ, Chen BP. ATR-dependent phosphorylation of DNA-dependent protein kinase catalytic subunit in response to UV-induced replication stress. Mol Cell Biol. 2006; 26:7520–7528. [PubMed: 16908529]

8. Hammel M, Yu Y, Mahaney BL, Cai B, Ye R, Phipps BM, et al. Ku and DNA-dependent protein kinase dynamic conformations and assembly regulate DNA binding and the initial non-homologous end joining complex. J Biol Chem. 2010; 285:1414–1423. [PubMed: 19893054]

9. Zhang S, Yajima H, Huynh H, Zheng J, Callen E, Chen HT, et al. Congenital bone marrow failure in DNA-PKcs mutant mice associated with deficiencies in DNA repair. J Cell Biol. 2011; 193:295–305. [PubMed: 21482716]

10. Mikkola HK, Orkin SH. The journey of developing hematopoietic stem cells. Development. 2006; 133:3733–3744. [PubMed: 16968814]

11. Mirchandani KD, D'Andrea AD. The Fanconi anemia/BRCA pathway: a coordinator of cross-link repair. Exp Cell Res. 2006; 312:2647–2653. [PubMed: 16859679]

12. McGowan KA, Li JZ, Park CY, Beaudry V, Tabor HK, Sabnis AJ, et al. Ribosomal mutations cause p53-mediated dark skin and pleiotropic effects. Nat Genet. 2008; 40:963–970. [PubMed: 18641651]

13. Nishio N, Kojima S. Recent progress in dyskeratosis congenita. Int J Hematol. 2010; 92:419–424. [PubMed: 20882440]

14. Kirwan M, Dokal I. Dyskeratosis congenita: a genetic disorder of many faces. Clinical genetics. 2008; 73:103–112. [PubMed: 18005359]

15. Hockemeyer D, Palm W, Wang RC, Couto SS, de Lange T. Engineered telomere degradation models dyskeratosis congenita. Genes Dev. 2008; 22:1773–1785. [PubMed: 18550783]

16. He H, Wang Y, Guo X, Ramchandani S, Ma J, Shen MF, et al. Pot1b deletion and telomerase haploinsufficiency in mice initiate an ATR-dependent DNA damage response and elicit phenotypes resembling dyskeratosis congenita. Mol Cell Biol. 2009; 29:229–240. [PubMed: 18936156]

17. Bailey SM, Cornforth MN, Kurimasa A, Chen DJ, Goodwin EH. Strand-specific postreplicative processing of mammalian telomeres. Science. 2001; 293:2462–2465. [PubMed: 11577237]

18. Gilley D, Tanaka H, Hande MP, Kurimasa A, Li GC, Oshimura M, et al. DNA-PKcs is critical for telomere capping. Proc Natl Acad Sci U S A. 2001; 98:15084–15088. [PubMed: 11742099]

19. Goytisolo FA, Samper E, Edmonson S, Taccioli GE, Blasco MA. The absence of the dna-dependent protein kinase catalytic subunit in mice results in anaphase bridges and in increased telomeric fusions with normal telomere length and G-strand overhang. Mol Cell Biol. 2001; 21:3642–3651. [PubMed: 11340158]

20. Jiang W, Crowe JL, Liu X, Nakajima S, Wang Y, Li C, et al. Differential phosphorylation of DNA-PKcs regulates the interplay between end-processing and end-ligation during nonhomologous end-joining. Mol Cell. 2015; 58:172–185. [PubMed: 25818648]

21. Williams ES, Klingler R, Ponnaiya B, Hardt T, Schrock E, Lees-Miller SP, et al. Telomere dysfunction and DNA-PKcs deficiency: characterization and consequence. Cancer Res. 2009; 69:2100–2107. [PubMed: 19244120]

22. Ishii-Ohba H, Kobayashi S, Nishimura M, Shimada Y, Tsuji H, Sado T, et al. Existence of a threshold-like dose for gamma-ray induction of thymic lymphomas and no susceptibility to radiation-induced solid tumors in SCID mice. Mutat Res. 2007; 619:124–133. [PubMed: 17397880]

23. de Lange T. Shelterin: the protein complex that shapes and safeguards human telomeres. Genes Dev. 2005; 19:2100–2110. [PubMed: 16166375]

24. Hultdin M, Gronlund E, Norrback KF, Eriksson-Lindstrom E, Just T, Roos G. Telomere analysis by fluorescence in situ hybridization and flow cytometry. Nucleic Acids Research. 1998; 26:3651–3656. [PubMed: 9685479]

25. Laud PR, Multani AS, Bailey SM, Wu L, Ma J, Kingsley C, et al. Elevated telomere-telomere recombination in WRN-deficient, telomere dysfunctional cells promotes escape from senescence and engagement of the ALT pathway. Genes Dev. 2005; 19:2560–2570. [PubMed: 16264192]

26. Hsu FM, Zhang S, Chen BP. Role of DNA-dependent protein kinase catalytic subunit in cancer development and treatment. Translational cancer research. 2012; 1:22–34. [PubMed: 22943041]

27. Wang X, Szabo C, Qian C, Amadio PG, Thibodeau SN, Cerhan JR, et al. Mutational analysis of thirty-two double-strand DNA break repair genes in breast and pancreatic cancers. Cancer Res. 2008; 68:971–975. [PubMed: 18281469]

28. Convery E, Shin EK, Ding Q, Wang W, Douglas P, Davis LS, et al. Inhibition of homologous recombination by variants of the catalytic subunit of the DNA-dependent protein kinase (DNA-PKcs). Proc Natl Acad Sci U S A. 2005; 102:1345–1350. [PubMed: 15668400]

29. Espejel S, Franco S, Sgura A, Gae D, Bailey SM, Taccioli GE, et al. Functional interaction between DNA-PKcs and telomerase in telomere length maintenance. Embo J. 2002; 21:6275–6287. [PubMed: 12426399]

30. Espejel S, Martin M, Klatt P, Martin-Caballero J, Flores JM, Blasco MA. Shorter telomeres, accelerated ageing and increased lymphoma in DNA-PKcs-deficient mice. EMBO Rep. 2004; 5:503–509. [PubMed: 15105825]

31. Ruis BL, Fattah KR, Hendrickson EA. DNA-PKcs Regulates Proliferation, Telomere Length and Genomic Stability in Human Somatic Cells. Mol Cell Biol. 2008

32. Chai W, Du Q, Shay JW, Wright WE. Human telomeres have different overhang sizes at leading versus lagging strands. Mol Cell. 2006; 21:427–435. [PubMed: 16455497]

33. Chow TT, Zhao Y, Mak SS, Shay JW, Wright WE. Early and late steps in telomere overhang processing in normal human cells: the position of the final RNA primer drives telomere shortening. Genes Dev. 2012; 26:1167–1178. [PubMed: 22661228]

34. Zhao Y, Sfeir AJ, Zou Y, Buseman CM, Chow TT, Shay JW, et al. Telomere extension occurs at most chromosome ends and is uncoupled from fill-in in human cancer cells. Cell. 2009; 138:463–475. [PubMed: 19665970]

35. Wu P, van Overbeek M, Rooney S, de Lange T. Apollo contributes to G overhang maintenance and protects leading-end telomeres. Mol Cell. 2010; 39:606–617. [PubMed: 20619712]

36. Verdun RE, Crabbe L, Haggblom C, Karlseder J. Functional human telomeres are recognized as DNA damage in G2 of the cell cycle. Mol Cell. 2005; 20:551–561. [PubMed: 16307919]

37. Sui J, Lin YF, Xu K, Lee KJ, Wang D, Chen BP. DNA-PKcs phosphorylates hnRNP-A1 to facilitate the RPA-to-POT1 switch and telomere capping after replication. Nucleic Acids Res. 2015; 43:5971–5983. [PubMed: 25999341]

38. Wang Y, Ghosh G, Hendrickson EA. Ku86 represses lethal telomere deletion events in human somatic cells. Proc Natl Acad Sci U S A. 2009; 106:12430–12435. [PubMed: 19581589]

39. Hayashi MT, Cesare AJ, Fitzpatrick JAJ, Lazzerini-Denchi E, Karlseder J. A telomere-dependent DNA damage checkpoint induced by prolonged mitotic arrest. Nature Structural & Molecular Biology. 2012; 19:387–394.

40. Bombarde O, Boby C, Gomez D, Frit P, Giraud-Panis MJ, Gilson E, et al. TRF2/RAP1 and DNA-PK mediate a double protection against joining at telomeric ends. EMBO J. 2010; 29:1573–1584. [PubMed: 20407424]

41. Khadka P, Lee JH, Baek SH, Oh SY, Chung IK. DNA-PKcs-interacting protein KIP binding to TRF2 is required for the maintenance of functional telomeres. Biochem J. 2014; 463:19–30. [PubMed: 25012820]

42. Karlseder J, Hoke K, Mirzoeva OK, Bakkenist C, Kastan MB, Petrini JH, et al. The telomeric protein TRF2 binds the ATM kinase and can inhibit the ATM-dependent DNA damage response. PLoS Biol. 2004; 2:E240. [PubMed: 15314656]

43. Giunta S, Belotserkovskaya R, Jackson SP. DNA damage signaling in response to double-strand breaks during mitosis. J Cell Biol. 2010; 190:197–207. [PubMed: 20660628]

44. Heijink AM, Krajewska M, van Vugt MA. The DNA damage response during mitosis. Mutat Res. 2013; 750:45–55. [PubMed: 23880065]

45. Orthwein A, Fradet-Turcotte A, Noordermeer SM, Canny MD, Brun CM, Strecker J, et al. Mitosis Inhibits DNA Double-Strand Break Repair to Guard Against Telomere Fusions. Science. 2014; 344:189–193. [PubMed: 24652939]

46. Yu H, Bauer B, Lipke GK, Phillips RL, Van Zant G. Apoptosis and hematopoiesis in murine fetal liver. Blood. 1993; 81:373–384. [PubMed: 7678514]

47. Poon, SS.; Lansdorp, PM. Quantitative fluorescence in situ hybridization (Q-FISH). In: Bonifacino, Juan S., et al., editors. Current protocols in cell biology / editorial board. Vol. Chapter 18. 2001. p. 14

48. Potts PR, Yu H. The SMC5/6 complex maintains telomere length in ALT cancer cells through SUMOylation of telomere-binding proteins. Nat Struct Mol Biol. 2007; 14:581–590. [PubMed: 17589526]

49. Schoenfeld DA. Sample-size formula for the proportional-hazards regression model. Biometrics. 1983; 39:499–503. [PubMed: 6354290]
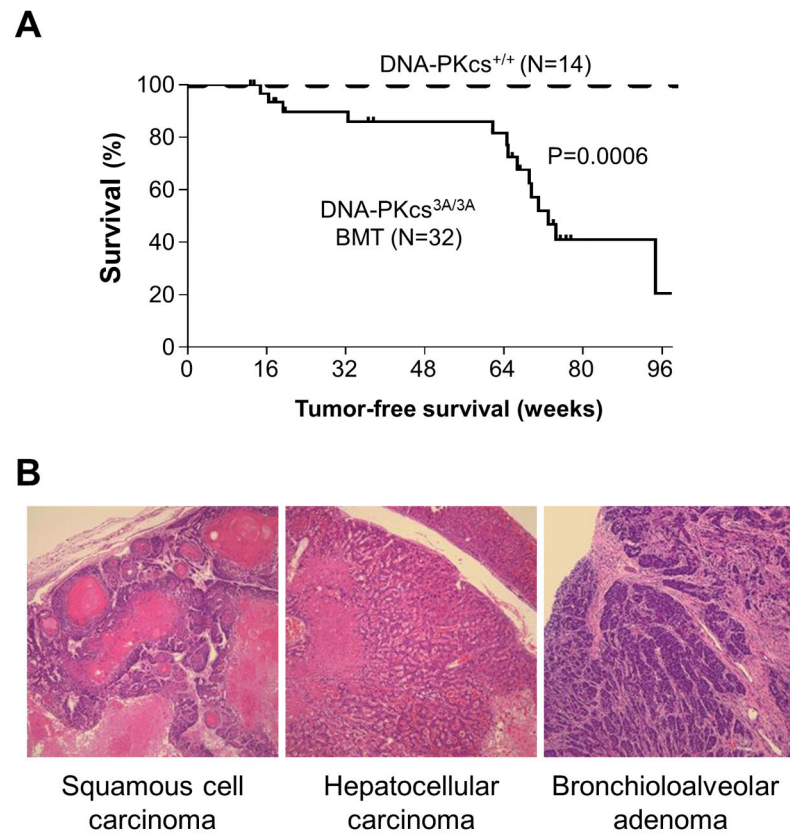
A

B

Squamous cell carcinoma

Hepatocellular carcinoma

Bronchioloalveolar adenoma

Figure 1. Tumor-prone phenotype of bone marrow transplantation-rescued DNA-PKcs[3A/3A] mice

(A) Tumor free survivals of BMT-rescued DNA-PKcs[3A/3A] and wild type control mice. BMT-rescued DNA-PKcs[3A/3A] mice display a significant increase in tumor incidence as compared to wild type control littermates. (B) Examples of tumor biopsy specimens stained with hematoxylin and eosin.
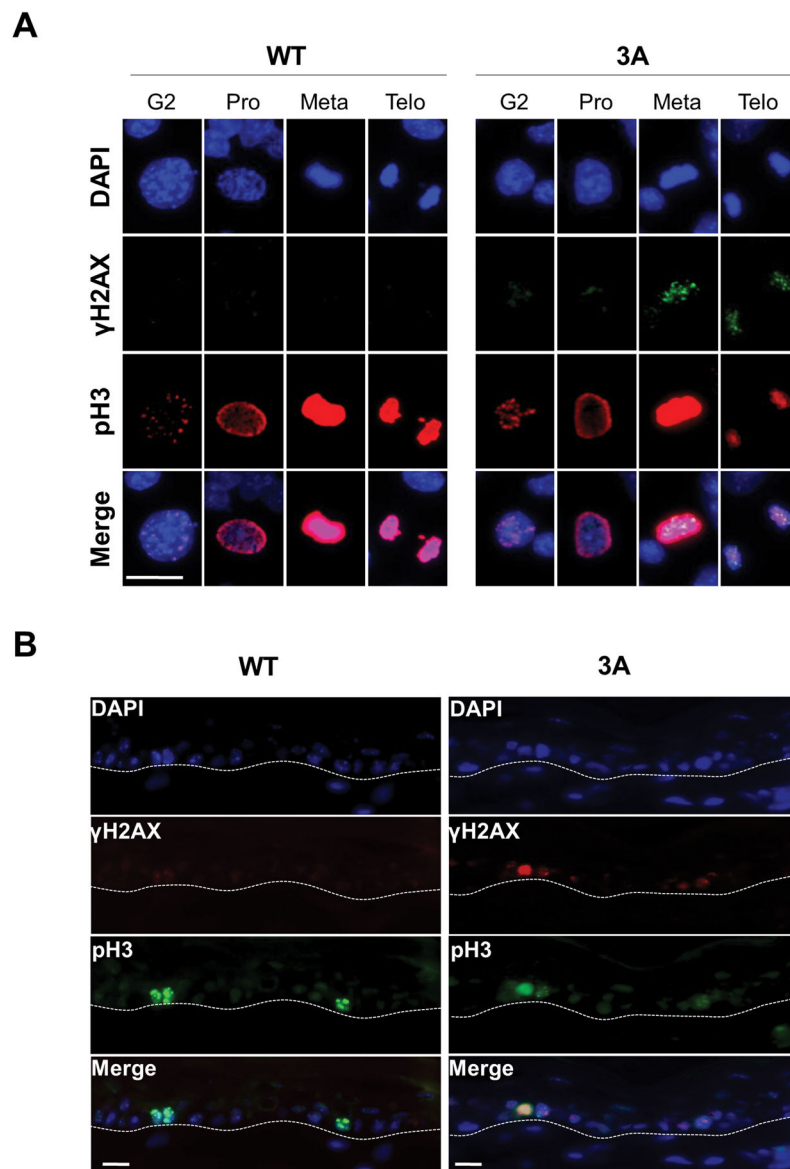
Figure 2. DNA-PKcs[3A/3A] keratinocytes display increased γH2AX staining during mitosis
(A) Freshly isolated skin keratinocytes were cultured and immunostained against γH2AX and phospho-histone 3 (pH3). γH2AX foci are visible in DNA-PKcs[3A/3A] keratinocytes during metaphase (meta) and telophase (telo), but not in prometaphase (prometa) and late G2 phase. Bar represents 10 μm. (B) Tail skin sections were prepared from postnatal day one pups and immunostained against γH2AX and pH3. A strong γH2AX staining signal was observed in DNA-PKcs[3A/3A] skin sections and overlapped with pH3 positive mitotic cells. Dashed lines indicate the base membrane.
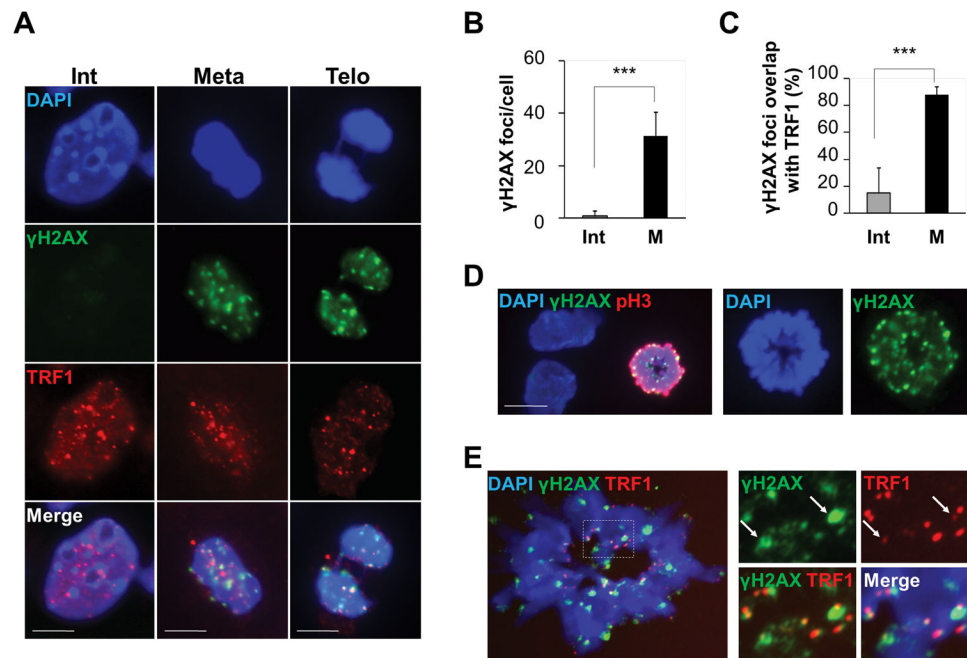
Figure 3. Mitosis specific γH2AX foci in DNA-PKcs$^{3A/3A}$ keratinocytes overlap with telomeres
(A) Primary DNA-PKcs$^{3A/3A}$ keratinocytes were immunostained against TRF1 and γH2AX. Significant γH2AX foci were found in mitotic cells (metaphase and telophase) but not in interphase cells (Int); they overlapped with TRF1 foci. Bar represents 10 μm. (B) Quantitation of γH2AX foci in DNA-PKcs$^{3A/3A}$ keratinocytes during interphase or mitosis. *** indicate P < 0.001. (C) Mitosis-induced γH2AX foci in DNA-PKcs$^{3A/3A}$ keratinocytes overlapped with TRF1 foci staining. The Mann-Whitney Rank Sum Test was used to compare two groups. A total of nine mitotic cell and nine interphase cells from three DNA-PKcs3A/3A mice were analyzed. (D) Fetal live hematopoietic stem cells (HSC) isolated from e12.5 DNA-PKcs$^{3A/3A}$ embryos were immunostained against mitotic marker pH3 and γH2AX. Bar represents 10 μm. (E) Overlapping of γH2AX and TRF1 staining in isolated fetal liver HSC during mitosis. Arrows indicate the inverse correlation between the intensities of γH2AX and TRF1 foci. Representative image of three independent experiments.
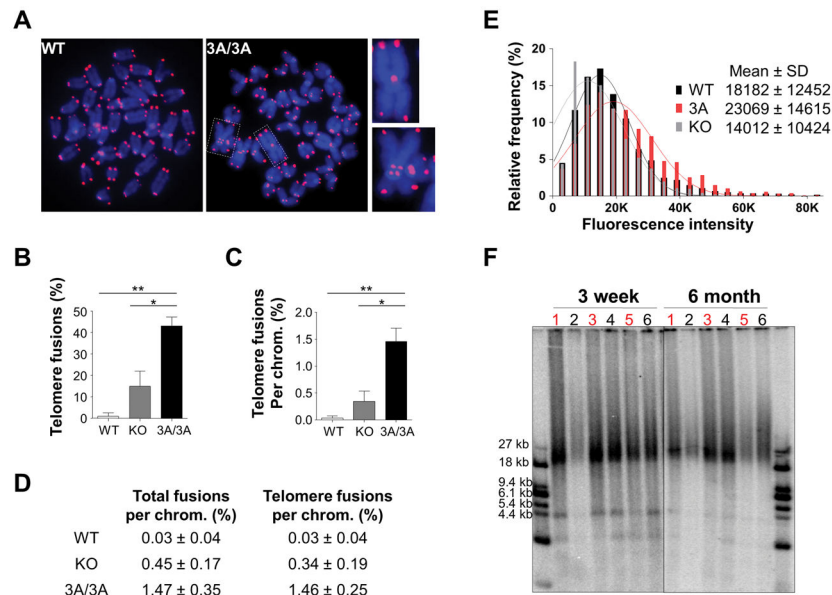
Figure 4. Increase of telomere fusion in DNA-PKcs[3A/3A] cells
(A) Representative telomere FISH image from wild type and DNA-PKcs[3A/3A] MEFs. Early passaged (>P5) primary MEFs underwent mitotic spread and Telomere FISH staining with TelC PNA probe (red) followed by chromosome counter-staining with DAPI (blue). (B–D) Telomere fusion analyses in wild type (WT), DNA-PKcs^{−/−} (KO), and DNA-PKcs[3A/3A] (3A/3A) MEFs. Frequencies of telomere fusion (B) and fusion frequencies per chromosome (C, D) were calculated from 100 mitotic spreads of each genotype from two independent experiments. *, P < 0.05; **, P < 0.01. (E) Quantitative fluorescence in situ hybridization (Q-FISH) of relative telomere lengths in wild type, DNA-PKcs^{−/−}, and DNA-PKcs[3A/3A] MEFs. Q-FISH was analyzed by the TFL-Telo software program [47]. (F) Genomic DNA isolated from skin samples of 3-week-old and 6-month-old wild type mice (black labels) or DNA-PKcs[3A/3A] (red labels) mice was digested, resolved in pulse field gel electrophoresis, and analyzed by Southern hybridization with ^{32}P-labeled (CCCTAA)$_3$ oligonucleotides to determine telomere length. Odd sample numbers in red represent DNA samples of DNA-PKcs[3A/3A] mice. Three individual DNA samples from each group were analyzed.
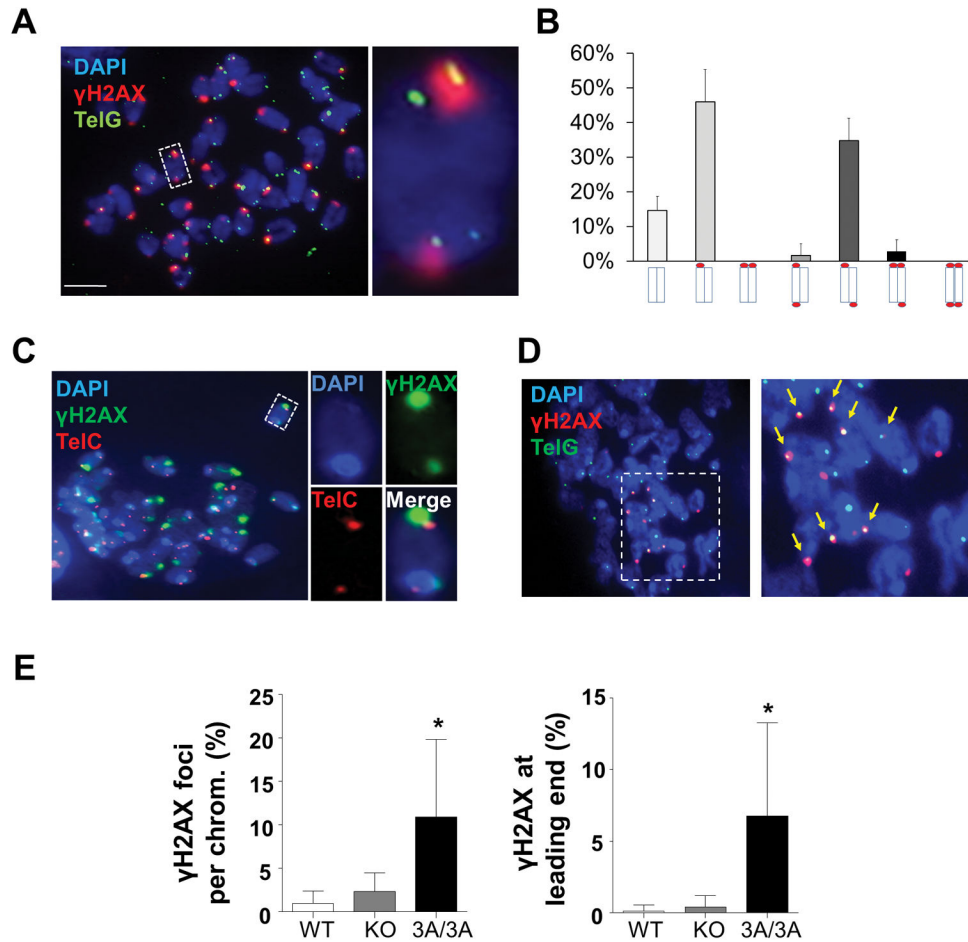
Figure 5. Leading strand telomere DNA damage in DNA-PKcs[3A/3A] cells

(A) Primary DNA-PKcs[3A/3A] skin fibroblasts were treated with 0.2 µg/ml colcemid for 30 minutes, prepared for mitotic spread, immunostained against γH2AX (red), and followed by fluorescence in situ hybridization (FISH) against a TelG-FITC PNA probe (green). Bar represents 5 µm. (B) Frequencies and distinctive patterns of γH2AX foci appearance among mitotic sister chromatids. The result was generated from two independent experiments with over 200 chromosomes analyzed each time. (C) Primary DNA-PKcs[3A/3A] skin fibroblasts were cultured with BrdU and BrdC for 16–20 hours, prepared for mitotic spread, immunostained against γH2AX (green), and processed for chromosome orientation-FISH (CO-FISH) with TelC-Cy3 PNA probe to label the lagging strand telomere synthesis (red). (D) The same procedure was performed to detect γH2AX (red) and leading strand telomere synthesis with TelG-FITC PNA probe (green). Arrows indicate the overlap between γH2AX and TelG staining. (E) Quantification of γH2AX foci overlapped with telomere leading strand synthesis in wild type, DNA-PKcs$^{-/-}$, and DNA-PKcs[3A/3A] MEFs. Over 50 mitotic cells were analyzed for each genotype. *, P < 0.05.
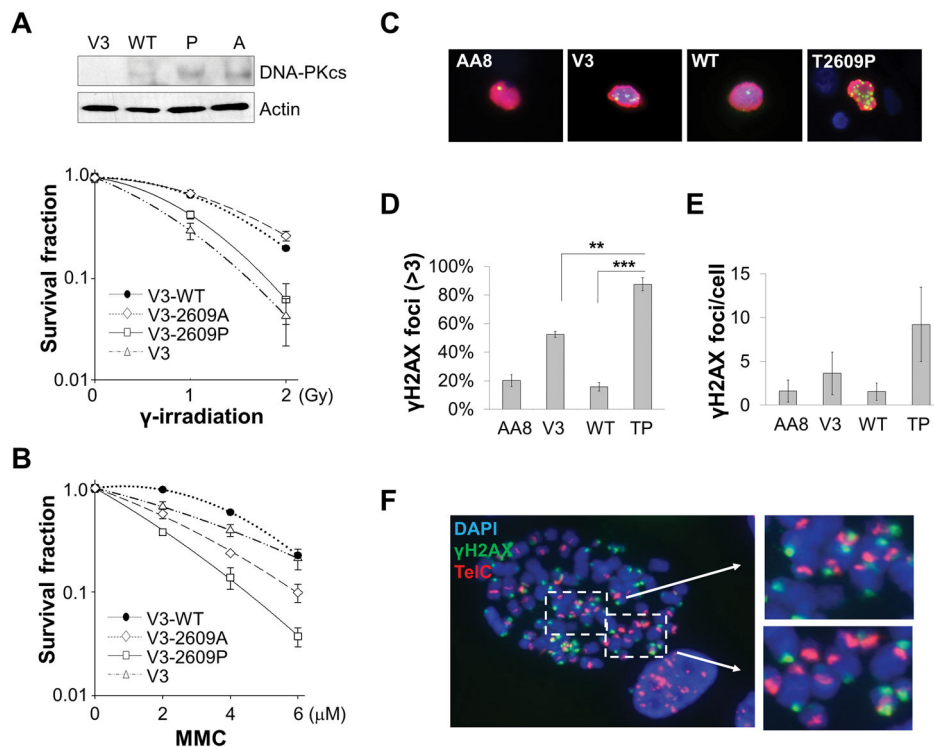
Figure 6. A Thr2609Pro missense variant of human DNA-PKcs causes leading strand telomere deprotection

(A) DNA-PKcs deficient CHO-V3 cells complemented with wild type DNA-PKcs (V3-WT) or mutant DNA-PKcs harboring T2609A (V3-T2609A) or T2609P (V3-T2609P) mutations were subjected to clonogenic survival analysis against γ-rays. The top panel shows expression levels of DNA-PKcs in different cell lines. (B) The same cell lines were analyzed for clonogenic survival analysis with mitomycin C. (C) Wild type CHO AA8 cells, CHO-V3, V3-WT, and V3-T2609P cells were immunostained against pH3 (red) and γH2AX (green). (D, E) Mitotic cell populations (pH3 positive) were analyzed for significant γH2AX foci (>3 foci per cell) (D) and the average number of γH2AX foci per cell (E). Results were generated from two independent experiments. **, P < 0.01; ***, P < 0.001. (F) V3-T2609P mutant cells were subjected to γH2AX staining (green) and CO-FISH assay against TelC-Cy3 probe (Red). Note that CHO cells have an interstitial telomeric sequence and display a telomere band staining pattern in telomere FISH analysis.

Table 1

Spontaneous tumor development in DNA-PKcs$^{3A/3A}$ BMT rescued mice.

ID	Age (weeks)	Tumor location	Histological diagnosis
C398	15	Thymus	Lymphoma
F522	16	Spleen	Lymphoma
F552	19	Spleen	Lymphoma
F518	32	Thymus	Lymphoma
F543	62	Liver	Hepatocellular carcinoma
C526	65	Liver	Hepatocellular carcinoma
F517	65	Head & Neck	Squamous cell carcinoma
C507	67	Head & Neck	Squamous cell carcinoma
C502	69	Back skin	Squamous cell carcinoma
F516	70	Hind leg	Spindle cell sarcoma
C375	71	Lung	Bronchioalveolar adenoma
C527	73	Head & Neck	Squamous cell carcinoma
C354	75	Head & Neck	Squamous cell carcinoma
C525	95	Liver	Hepatocellular carcinoma